Polarizability of Rn-like Th^{4+} from spectroscopy of high-L Rydberg levels of Th^{3+}

M. E. Hanni, Julie A. Keele, and S. R. Lundeen
Department of Physics, Colorado State University, Fort Collins, Colorado 80523, USA

C. W. Fehrenbach
J. R. Macdonald Laboratory, Kansas State University, Manhattan, Kansas 66506, USA

(Received 7 July 2010; published 25 August 2010)

Binding energies of high-L Rydberg levels of Th^{3+} were measured using the resonant excitation Stark ionization spectroscopy technique. Analysis of the data with the long-range polarization model leads to determination of dipole and quadrupole polarizabilities of the free Th^{4+} ion, $\alpha_d = 7.61(6)$ a.u., $\alpha_Q = 47(11)$ a.u.

DOI: 10.1103/PhysRevA.82.022512 PACS number(s): 32.30.Bv, 32.10.Dk, 32.10.Fn

I. INTRODUCTION

The Th^{4+} ion is a closed-shell Radon-like ion with a ground-state configuration of $6p^6\,{}^1S_0$. It is the most common charge state of Th in chemical compounds [1]. The lowest excited states of this ion are believed to be $6p^5 5f$ levels with excitation energies in the range 17–20 eV [2], but no optical spectroscopy exists for this ion [3]. The most significant dynamic properties of Th^{4+} are its dipole and quadrupole polarizabilities. Experimental measurement of these properties can begin to test the various theoretical methods used to describe this highly relativistic multielectron ion. Such descriptions are of course imbedded in the even more complex calculations used to describe the chemistry of Th and of other actinide elements.

The polarizabilities of Th^{4+} can be measured by attaching a single electron to the Th^{4+} ion in a highly excited, nonpenetrating Rydberg state. The binding energy of such a Rydberg electron depends slightly on its orbital angular momentum, and measurement of the Rydberg electron's binding energy across a range of high-L levels can be used to determine the polarizabilities of the ion binding it. A general method for forming and studying such high-L Rydberg levels is provided by the resonant excitation Stark ionization spectroscopy (RESIS) technique. A fast beam of the ion of interest ($v/c \sim 0.001$) captures a single electron from a dense Rydberg target. Resonant charge transfer results in capture into very highly excited levels of the Rydberg ion. These can be further excited by a Doppler-tuned CO_2 laser, and this excitation can be detected by Stark ionization of the upper level. The frequency resolution of the CO_2 excitation is sufficient to partially resolve the binding energies of a range of high-L levels, giving a measurement of the ion polarizability. This technique is easily adapted to different elements and different charge states and has been used in the past for a wide range of studies [4].

II. EXPERIMENT

This study is carried out with the same apparatus used recently to determine the polarizabilities of Pb^{2+} and Pb^{4+} by the RESIS method [5]. A beam of Th^{4+} ions is extracted by sputtering Th metal in a 14-GHz permanent magnet electron cyclotron resonance ion source. The beam is accelerated to approximately 100 keV, mass and charge selected in a 20° magnet, and focused through a 2-mm-diam aperture by two pairs of electric quadrupole doublet lenses. There it intersects the Rydberg target, a thermal beam of Rb excited to the $10F$ level by three continuous-wave lasers. A few percent of the Th^{4+} ions capture an electron to become highly excited Rydberg states of Th^{3+}, and these are then charge selected by a 15° bending magnet. The Rydberg Th^{3+} beam passes through two einzel lenses, which focus the beam and ionize any very weakly bound Rydberg levels, and then passes through the CO_2 laser beam. The CO_2 laser line is selected to nearly match a possible upward transition between Rydberg levels of Th^{3+} and is fine-tuned by varying the angle of intersection between the fixed-frequency CO_2 laser and the fast ion beam. Table I lists the transitions and laser lines used in this study. When the Doppler-tuned laser frequency is resonant with an upward transition, very highly excited Rydberg ion levels are produced. These are detected by Stark ionization and collection of the resulting Th^{4+} ions. Figure 1 shows the RESIS spectra obtained in this study for the first transition listed in Table I. The horizontal axis in Fig. 1 gives the difference between the Doppler-tuned laser frequency and the nonrelativistic hydrogenic transition frequency for the transition. The sequence of resolved lines corresponds to excitation of $L = 10$, 9, 8, and 7 levels in $n = 37$, as indicated in Fig. 1.

The clear pattern of line positions displayed in Fig. 1 is not, in itself, sufficient to provide identification of the resolved lines. If an approximate value of the dipole polarizability is known, accurate to within a factor of 2, this can be used to identify the lines using the effective potential model discussed below. Sometimes, such an initial estimate of α_d can be obtained by study of Rydberg series of lower L in Rydberg states whose core is the ion in question. This approach was used successfully in the recent study of Pb^{2+} and Pb^{4+} [5]. Since very little optical spectrosopy of Th^{3+} is available [3], the line identifications shown in Fig. 1 were obtained from a theoretical estimate of the Th^{4+} polarizability. Safronova calculated a polarizability of 7.75 a.u. [6] and suggested that this estimate was probably accurate to 5%, which is more than adequate to identify the lines. Although optical spectroscopy of Th^{3+} is very sparse, the location of the $5g$ level and the Th^{3+} ionization energy have been reported [7] and these data confirm the line identifications, as discussed below.

The laser is Doppler tuned by reflecting it from a rotatable mirror mounted on a computer-controlled rotation stage. The resulting frequency in the rest frame of the Rydberg ion

TABLE I. Specific RESIS transitions used in this study and the CO_2 laser lines used to excite them.

Transition $(n.n')$	E_0[a] (cm^{-1})	CO_2 line	E_L (cm^{-1})
(37, 73)	953.057 7	$10P(10)$	952.880 9
(38, 79)	934.590 8	$10P(30)$	934.894 5
(37, 76)	978.556 1	$10R(24)$	978.472 3

[a]Column 2 shows, in each case, the nonrelativistic hydrogenic transition energy.

depends on the speed of the ion and the angle of intersection between the laser and ion beam:

$$\nu_L' = \frac{\nu_L}{\sqrt{1-\beta^2}}(1+\beta\cos\theta_{\rm int}), \tag{1}$$

where β is the speed of the beam in units of c and $\theta_{\rm int}$ is the angle of intersection, determined from

$$\theta_{\rm int} = 90^\circ - 2(\theta_{\rm obs} - \theta_\perp), \tag{2}$$

where $\theta_{\rm obs}$ is the reading of the rotation stage and $\theta_\perp$ is the angle at which the intersection is exactly 90°. For this study, β was determined by calibration of the acceleration potential and $\theta_\perp$ was determined by observation of a RESIS spectrum whose scale is precisely known from microwave spectroscopy [8]. The precision of $\theta_\perp$ is limited by the pointing stability of the ion beam. The values determined were

$$\beta = 0.000\,9608(10), \quad \theta_\perp = 1.08(1)^\circ.$$

The uncertainties in these two constants were the primary source of uncertainty in the line positions reported here.

Table II lists the transitions used for this study and reports the value of $\theta_{\rm int}$ at which they were observed and the corresponding value of ΔE, the difference of the transition frequency from the hydrogenic frequency. The uncertainties shown there include only the statistical uncertainties from fitting the resonance lines and not the uncertainties due to

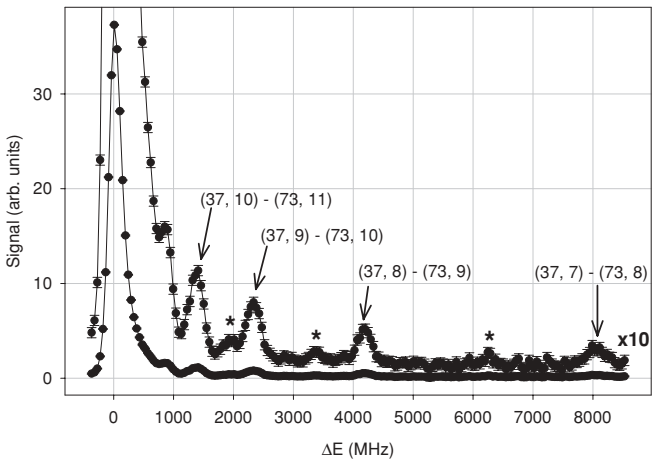

FIG. 1. RESIS excitation spectrum of the $n = 37$–73 transition in Th^{3+}. The x axis represents the energy difference from the hydrogenic energy of the 37–73 transition. The 10× magnified plot allows a better view of the resolved signals. The asterisks indicate $\Delta L = -1$ transitions.

TABLE II. Resolved RESIS transitions observed in this study.

Transition	Number of observations[d]	$\theta_{\rm int}$[a] (deg)	$\Delta E^{\rm Stark}$[b] (MHz)	$\Delta E^{\rm obs}$[c] (MHz)
(37,10)-(73,11)	16	75.850(24)	1(1)	1414(11)
(37,9)-(73,10)	16	73.848(24)	1(1)	2340(11)
(37,8)-(73,9)	16	69.786(18)	1(1)	4188(8)
(37,7)-(73,8)	8	60.918(58)	−2(2)	8048(24)
(37,7)-(76,8)	3	67.926(86)	−1(1)	8095(39)
(38,10)-(79,11)	18	106.776(28)	1(1)	1334(13)
(38,9)-(79,10)	21	104.894(26)	2(2)	2814(12)
(38,8)-(79,9)	16	101.168(34)	3(3)	3889(16)

[a]Averaged intersection angle of the transition in column 1.
[b]Small Stark shift correction applied.
[c]Energy difference of the observed transition from the hydrogenic energy of the transition. The error reported on the measurement is the statistical error resulting from the error in the determination of the intersection angle listed in column 3.
[d]Number of independent observations of the transition in column 1.

β and $\theta_\perp$. In general, upward transitions are allowed for two possible values of upper state angular momentum, $\Delta L = \pm 1$. The $\Delta L = 1$ is the stronger transition, and the only one which we use in the analysis that follows. The weaker $\Delta L = -1$ transitions occur at slightly lower values of ΔE and are indicated in Fig. 1 by asterisks. When the primary $\Delta L = 1$ line was well resolved it was fit to a single Gaussian function to extract the line position. For the initial states with $L \geqslant 9$, where the weaker $\Delta L = -1$ transition was not completely resolved, the composite line was fit to a superposition of two Gaussians with the strength and relative position of the weaker line fixed by study of the better resolved cases.

Another experimental issue is the possible effect of stray electric fields within the laser interaction region, which could cause Stark shifts in the upper state of the transition. By studying the widths of the RESIS transitions, and especially the variation in width with angular momentum, it was determined that the stray field was $\leqslant 0.05$ V/cm. The effect of fields of this size is very nearly negligible for this study. The predicted effect was calculated by diagonalizing the Stark Hamiltonian of the upper state and simulating the expected RESIS transition as a function of stray field. A small correction and uncertainty were applied to each line position based on these studies. Table II shows the applied Stark corrections. The final column of Table II represents the interval in the absence of Stark shifts.

III. ANALYSIS AND RESULTS

The deviation of the individual line positions from the hydrogenic value is primarily due to the polarization energies in the upper and lower levels of the transition. The polarization energy is the expectation value of an effective potential,

$$V_{\rm eff} = -\frac{\alpha_{\rm d}}{2r^4} - \frac{(\alpha_{\rm Q} - 6\beta_{\rm d})}{2r^6} + \cdots, \tag{3}$$

in which the coefficients are properties of the Th^{4+} core: dipole ($\alpha_{\rm d}$) and quadrupole ($\alpha_{\rm Q}$) polarizabilities and the nonadiabatic dipole polarizability ($\beta_{\rm d}$). For reference, expressions for each of these core properties are reproduced in the Appendix. Two

TABLE III. List of the small corrections applied to determine the first-order energy differences arising from the long-range interaction of the Rydberg electron with the Th^{4+} ion core from the measured frequency offsets. Columns 1 and 2 are reproduced from Table II for reference; columns 3 and 4 represent the small energy contributions arising from the second-order and relativistic energies; and column 5 gives the portion of the energy offset $\Delta E^{\rm obs}$ that is due to the expectation value of $V_{\rm eff}$.

Transition (n,L)-(n',L')	$\Delta E^{\rm obs}$ (MHz)	$\Delta E^{[2]}$ (MHz)	$\Delta E^{\rm rel}$ (MHz)	$\Delta E^{[1]}$ (MHz)
(37,10)-(73,11)	1415(11)	0.876(14)	57.5	1356(11)
(37,9)-(73,10)	2341(11)	2.695(43)	65.5	2272(11)
(37,8)-(73,9)	4189(8)	9.403(149)	75.3	4103(8)
(37,7)-(73,8)	8046(24)	38.479(364)	87.7	7922(24)
(37,7)-(76,8)	8094(39)	38.504(365)	89.1	7967(39)
(38,10)-(79,11)	1335(13)	0.816(13)	54.7	1279(13)
(38,9)-(79,10)	2186(12)	2.508(40)	62.1	2119(12)
(38,8)-(79,9)	3892(16)	8.739(139)	71.3	3809(16)

other smaller contributions to the Rydberg energies are due to relativistic corrections, $E^{\rm rel}$, and second-order corrections, $E^{[2]}$. The relativistic correction is the hydrogenic value coming from the p^4 correction to the Rydberg electron's kinetic energy. The second-order correction comes from applying $V_{\rm eff}$ in second order and has been calculated analytically by Drake and Swainson if only the leading term proportional to $\alpha_{\rm d}^2$ is included [9]. By removing the small contributions from these two terms, the dominant effect, due to the expectation value of $V_{\rm eff}$, is isolated, simplifying the subsequent analysis. Table III shows the reduction of the measured line positions to the difference of the expectation values of $V_{\rm eff}$ in the upper and lower levels of the transition:

$$\Delta E^{[1]} = \Delta E^{\rm obs} - \Delta E^{\rm rel} - \Delta E^{[2]}. \tag{4}$$

A scaled plot should remove most of the variation of $\Delta E^{[1]}$ with n and L and yield estimates of the core parameters occurring in $V_{\rm eff}$:

$$\frac{\Delta E^{[1]}}{\Delta\langle r^{-4}\rangle} = \frac{\alpha_{\rm d}}{2} + \frac{(\alpha_{\rm Q} - 6\beta_{\rm d})}{2}\frac{\Delta\langle r^{-6}\rangle}{\Delta\langle r^{-4}\rangle} + \cdots = A_4 + A_6\frac{\Delta\langle r^{-6}\rangle}{\Delta\langle r^{-4}\rangle} + \cdots, \tag{5}$$

Figure 2 shows such a scaled plot. It is completely consistent with the linear trend expected if higher terms in $V_{\rm eff}$ are negligible. The fit returns the following parameters:

$$A_4 = 3.806(30), \quad A_6 = 13.0(2.1).$$

The fitted value of A_4 gives the dipole polarizability of Th^{4+}:

$$\alpha_{\rm d} = 7.61(6)\ \text{a.u.}$$

The coefficient $\beta_{\rm d}$ is related to the same dipole transition strengths between the ground and excited states of Th^{4+} that determine $\alpha_{\rm d}$. If $\alpha_{\rm d}$ were entirely due to excitation to a single level with excitation $\Delta E_{\rm core}$, then $\beta_{\rm d}$ would be simply related

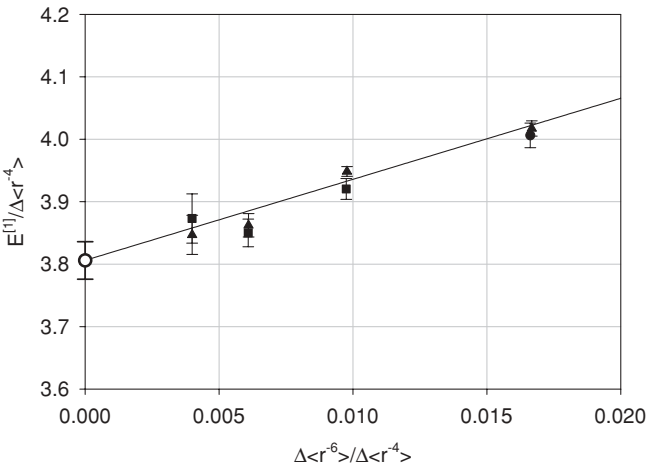

FIG. 2. Plot of the scaled first-order polarization energies in Th^{3+}. The triangles represent the scaled energies determined from the 37–73 transitions, the circle represents the scaled energy of the (37,7)–(76,8) transition, and the squares represent the scaled energies determined from the 38–79 transitions. The vertical axis represents the ratio of the first-order polarization energies to the difference of expectation values of r^{-4} in the upper and lower state of the transition. The horizontal axis represents the ratio of the expectation value differences of r^{-6} to r^{-4}. The solid line represents the fit of all the data to the linear form predicted by the long-range polarization model. The open circle indicates the intercept, determining the dipole polarizability. All energies and lengths are in atomic units.

to $\alpha_{\rm d}$ by

$$\beta_{\rm d} = \frac{\alpha_{\rm d}}{2\Delta E_{\rm core}}. \tag{6}$$

However, knowing only the total polarizability, without knowledge of which excited levels contribute to it and what their excitation energies are, gives only a crude estimate of $\beta_{\rm d}$. Theoretical estimates [2] place the lowest dipole excited level of Th^{4+} at about 20 eV (0.735 a.u.) and the ionization energy at 58 eV (2.13 a.u.). If we assume that most of the dipole transition strength comes from bound levels of Th^{4+}, we can crudely estimate that $1.8 \leqslant \beta_{\rm d} \leqslant 5.2$. This allows an estimate of the quadrupole polarizability $\alpha_{\rm Q}$ from the measured parameter A_6:

$$\alpha_{\rm Q} = 2A_6 + 6\beta_{\rm d} = 26(4) + 21(10) = 47(11)\ \text{a.u.} \tag{7}$$

Such a large value of $\alpha_{\rm Q}$ is consistent with the fact that the lowest excited levels of Th^{4+} are $6p^5 4f$ levels that would be quadrupole excited. It would, of course, be preferable to have a more precise estimate of $\beta_{\rm d}$, making possible a more precise estimate of $\alpha_{\rm Q}$ from the fitted parameter A_6. An alternative approach would be to compare A_6 directly to the proper linear combination of the two calculated core parameters $\alpha_{\rm Q}$ and $\beta_{\rm d}$.

Optical spectroscopy of Th^{3+} has established the excitation energy of the $5g$ level (159,379 cm^{-1}) and the Th^{3+} ionization energy [231,065 (242) cm^{-1}] [7]. Although the $5g$ level may not be precisely described by the long-range model, these two values suffice to place a point on a scaled plot similar to Fig. 2

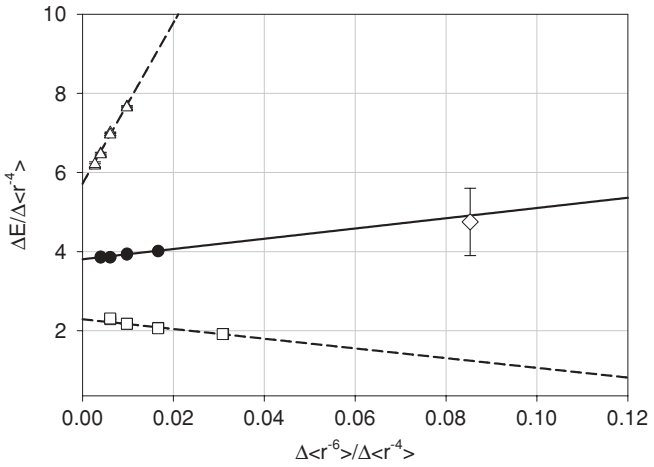

FIG. 3. Plot of the scaled first-order polarization energies of Th^{3+}, assuming three possible identifications of the transitions shown in Fig. 1. The solid circles represent the scaled energies of the transitions as identified in Fig. 1, and the solid line represents the extrapolated fit of the long-range polarization model to the solid circles. The open triangles represent the scaled energies if the L's of the identified transitions are all increased by 1 unit. The open squares represent the scaled energies if the L's of the identified transitions are all decreased by 1 unit. The dashed lines represent linear fits to the open triangles and squares. The open diamond represents the scaled first-order energy of the $5g$ state observed by Klinkenberg [7]. This point is consistent with the extrapolation of linear fit using the chosen line identifications but not with the alternate identifications.

corresponding to the $5g$ level:

$$E_{5g}^{[1]} = E_{5g} - E_I + \frac{\mathcal{R}_M}{5^2} - E_{5g}^{[2]}. \tag{8}$$

Figure 3 shows such a plot, including the points from Fig. 2 as solid circles and the analogous scaled points that would result if the line identifications were shifted by one unit up or down in L by open triangles or squares, respectively. All three cases are consistent with linear fits, also shown in Fig. 3, but with widely varying intercepts and slopes. The single point corresponding to the scaled energy of the $5g$ level is shown in Fig. 3 as an open diamond. It is completely consistent with the fitted line from the polarization plot of Fig. 2, shown as a solid line in Fig. 3, but inconsistent with the linear fits corresponding to the two alternate line identifications. This confirms the line identifications of Fig. 1. The uncertainty in the $5g$ point is due primarily to uncertainty in the ionization energy of Th^{3+}. If the applicability of the long-range model to the $5g$ level were more certain, or if the positions of more and higher L levels of Th^{3+} were known, this analysis could improve the precision of the Th^{3+} ionization energy. An additional reason for rejecting the alternate identifications in Fig. 3 is the physically unreasonable values of α_Q that they would imply.

IV. DISCUSSION

Table IV summarizes the Th^{4+} properties determined by this study and compares them, when possible, with theoretical predictions. Calculations of dipole polarizabilities have been reviewed recently by Mitroy *et al.* [10]. For Th^{4+}, a range of theoretical predictions is available. The results from a Hartree-Fock (HF) calculation [11] and from a fully relativistic Dirac-Hartree-Fock (DHF) calculation [12] are shown for comparison. A result obtained with relativistic random phase approximation (RRPA) [6,12] is expected to be more accurate, with an estimated precision of 5%. It agrees with the experimental measurement to well within this precision. Agreement with the calculation of Borschevsky and Schwerdtfeger [13], obtained using a relativistic coupled-cluster method including single, double, and partial triple excitations RCCSD(T) [14] is also very good. It will be very interesting to compare the measured ion polarizability to predictions obtained with methods that are more typically used in descriptions of more complicated systems [15]. To date, we are unaware of any calculations of either β_d or α_Q.

TABLE IV. Comparison between the Th^{4+} properties determined in this study and the results of several theoretical calculations. All quantities are expressed in atomic units.

Quantity	Expt.	Theory	(Theory)/(Expt.)
α_d	7.61(6)	10.26 (HF)[a]	1.348(8)
		8.96 (DHF)[b]	1.177(8)
		7.75 (RRPA)[c]	1.018(8)
		7.699 (RCCSD(T))[d]	1.012(8)
α_Q-$6\beta_d$	26.0(4.2)		
β_d	3.5(1.7)[e]		
α_Q	47(11)		

[a]Fraga, Karwowski, and Saxena [10].
[b]Derevianko [11].
[c]Derevianko [11] and Safronova [6].
[d]Borschevsky and Schwerdtfeger [12].
[e]Estimated from α_d, as described in text.

Although Th^{4+} is a closed-shell ion, its polarizability is quite large. This suggests that valence-core correlations are significant in lower charge states of Th, such as Fr-like Th^{3+} and Ra-like Th^{2+}. Some calculations assessing the effects of such correlation directly input the Th^{4+} polarizability [16], and these are improved by use of the measured value.

The measurement technique used here should be applicable to other Rn-like ions, in particular Ra^{2+} and U^{6+}. It would be impractical with the more active Rn-like ions. Higher-precision measurements should be possible using microwave spectroscopy detected with the RESIS technique [17].

ACKNOWLEDGMENTS

The work reported here was carried out in the J. R. Macdonald Laboratory of Kansas State University. We are grateful for the cooperation of the laboratory staff and management. The work was supported by the Chemical Sciences, Geosciences, and Biosciences Division of the Office of Basic Energy Science, U.S. Department of Energy.

APPENDIX

The core properties that appear in the long-range potential are given by

$$\alpha_D = \frac{2}{3(2J+1)} \sum_{e,J'} \frac{|\langle g, J|D|eJ'\rangle|^2}{E(e,J')},$$

$$\beta_{\rm d} = \frac{1}{3(2J+1)} \sum_{e,J'} \frac{|\langle g,J|D|eJ'\rangle|^2}{E(e,J')^2},$$

$$\alpha_{\rm Q} = \frac{2}{5(2J+1)} \sum_{e,J'} \frac{|\langle g,J|Q|eJ'\rangle|}{E(eJ')},$$

where J and J' are the angular momenta of the ground and excited states, the sum is over all excited levels, and D and Q represent the dipole and quadrupole moment operators:

$$D \equiv \sum_{i=1}^{N1} r_i C^{[1]}(\Omega_i), \quad Q \equiv \sum_{i=1}^{N} r_i^2 C^{[2]}(\Omega_i).$$

[1] *The Chemistry of the Actinide and Transactinide Elements*, edited by L. R. Morss, N. M. Edelstein, and J. Fuger (Springer, Dordrecht, Netherlands, 2006).

[2] Donald Beck (private communication); U. Safronova (private communication).

[3] J. Blaise and J. F. Wyart [http://www.lac.u-psud.fr/Database/Contents.html].

[4] S. R. Lundeen, in *Advances in Atomic, Molecular, and Optical Physics*, edited by C. C. Lin and P. Berman (Academic, New York, 2005), pp. 161–208.

[5] M. E. Hanni, J. A. Keele, S. R. Lundeen, C. W. Fehrenbach, and W. G. Sturrus, Phys. Rev. A **81**, 042512 (2010).

[6] U. I. Safronova, W. R. Johnson, and M. S. Safronova, Phys. Rev. A **76**, 042504 (2007).

[7] P. F. A. Klinkenberg, Physica B + C (Utrecht) **151**, 552 (1988).

[8] R. A. Komara, M. A. Gearba, C. W. Fehrenbach, and S. R. Lundeen, J. Phys. B **38**, S87 (2005).

[9] G. W. F. Drake and R. A. Swainson, Phys. Rev. A **44**, 5448 (1991).

[10] J. Mitroy, M. S. Safronova, and C. W. Clark, e-print arXiv:1004.3567.

[11] S. Fraga, J. Karwowski, and K. M. S. Saxena, *Handbook of Atomic Data* (Elsevier, Amsterdam, 1976).

[12] A. Derevianko (private communication).

[13] A. Borschevsky and P. Schwerdtfeger (private communication).

[14] I. S. Lim and P. Schwerdtfeger, Phys. Rev. A **70**, 062501 (2004).

[15] E. V. Beck *et al.*, J. Phys. Chem. A **113**, 12626 (2009).

[16] E. Biemont, V. Fivet, and P. Quinet, J. Phys. B **37**, 4193 (2004).

[17] R. A. Komara, M. A. Gearba, S. R. Lundeen, and C. W. Fehrenbach, Phys. Rev. A **67**, 062502 (2003).